ELSEVIER

Earth and Planetary Science Letters 183 (2000) 291–302

EPSL

www.elsevier.com/locate/epsl

U–Th dating of single zircons from young granitoid xenoliths: new tools for understanding volcanic processes

J.B. Lowenstern [a,*], H.M. Persing [b], J.L. Wooden [b], M. Lanphere [b], J. Donnelly-Nolan [a], T.L. Grove [c]

[a] *US Geological Survey, MS 910, 345 Middlefield Road, Menlo Park, CA 94025, USA*
[b] *US Geological Survey, MS 937, 345 Middlefield Road, Menlo Park, CA 94025, USA*
[c] *Department of Earth, Atmospheric and Planetary Science, Massachusetts Institute of Technology, Cambridge, MA 02139, USA*

Received 26 June 2000; received in revised form 11 September 2000; accepted 24 September 2000

Abstract

Multiple U–Th isotopic analyses of individual zircon crystals by ion microprobe define isochrons that discriminate between different crystallization ages of granitoid xenoliths in lavas erupted 1065 and 2000 years ago from Medicine Lake volcano, CA, USA. Zircon ages indicate at least two intrusive episodes, ~25 and ~90 ka, at times when silicic volcanism was rare, but basaltic volcanism was prevalent. Ar–Ar spectra require that the granitoids were completely crystalline thousands of years prior to their mobilization and eruption. These techniques demonstrate that individual zircon crystals can form rapidly enough to provide unique U–Th ages, and allow dating of <300 ka xenoliths from volcanic eruptions.

Keywords: zircon; U-238/Th-230; geochronology; ion probe data; SHRIMP data; Medicine Lake; California; granites xenolith

1. Introduction

Recent analytical advances now permit U–Th isotopic analysis of individual 30–50 μm spots on U and Th-rich crystals separated from igneous rocks, potentially dating crystallization events, up to and including eruption or intrusion [1,2]. In U–Th geochronology, ages are calculated either by pooled model ages [1], assuming an initial $^{230}Th/^{232}Th$ for the crystals, or by fitting analyses of multiple crystals with an isochron [2]. Ideally, it would be preferable to independently calculate the ages of individual crystals without the need to pool data or to assume an initial $^{230}Th/^{232}Th$ from a whole rock analysis [3]. One could then discriminate the age of each crystal and, thereby, assess the importance of mixing, assimilation and multiple crystallization events in the history of the host rock.

We present single crystal isochron ages for zircon ($ZrSiO_4$) crystals from granitoid xenoliths [2,4–7] erupted as inclusions within glassy, late Holocene rhyolitic and dacitic lava flows from Medicine Lake volcano (MLV, [8], 41°35′N, 121°35′W). As shown below, these xenoliths rep-

* Corresponding author. Tel.: +1-650-329-5238; Fax: +1-650-329-5203; E-mail: jlwnstrn@usgs.gov

0012-821X/00/$ – see front matter
PII: S0012-821X(00)00273-9

resent <150 ka intrusions related to MLV, but are significantly older than their host lavas. Using the Stanford-USGS, reverse geometry, sensitive high resolution ion microprobe (SHRIMP-RG), we conducted multiple U–Th isotopic analyses on individual crystals, producing isochrons that date their ages of formation. We find evidence for intrusion of at least two different shallow ($<\sim 6$ km) granitoids at ~ 90 ka and again at ~ 25 ka, periods dominated by mafic volcanism at MLV. Ar–Ar spectra indicate that the xenoliths were crystalline long before their eruption in the late Holocene.

2. Background and sample information

MLV is a Cascade volcano located about 60 km northeast of Mt. Shasta at the edge of the Basin and Range province, just south of the California–Oregon border [4,8–11]. Seventeen Holocene eruptions produced rhyolitic domes and some intermediate lavas vented in and near a central caldera, as well as basaltic to andesitic lavas erupted outside the caldera. The most recent volcanism produced the 885 ± 40 yr Glass Mountain rhyolite [8,11].

Unaltered granitoid xenoliths occur in many Holocene lava flows [4,8,10–12] and many Pleistocene units at MLV; the vents, and therefore the sampled granitoid intrusions, must underlie a region exceeding 150 km^2. The xenoliths are compositionally and isotopically diverse, consistent with the existence of a variety of small, shallow intrusions and dikes rather than a single large pluton [9]. Because Holocene rhyolites such as

Table 1
Sample information for granitoid xenoliths

Sample	MD1	MD2	CG1a	CG1b
Host lava	Medicine dacite	Medicine dacite	Crater Glass	Crater Glass
Field No.	86–3	680M	2050Ma	2050Mb
Host age[8]	~ 2000 yr	~ 2000 yr	1065 ± 90 yr	1065 ± 90 yr
Composition	granite	granite	granodiorite	diorite
SiO_2	72.1	73.0	63.8	56.3
Al_2O_3	14.7	13.9	17.0	16.9
Fe_2O_3*	2.08	1.65	4.65	7.89
MgO	0.49	0.40	1.44	3.64
CaO	1.35	1.47	3.82	6.63
Na_2O	3.71	3.73	4.43	4.64
K_2O	4.70	4.04	2.61	1.68
TiO_2	0.30	0.22	0.79	1.06
P_2O_5	0.07	0.09	0.23	0.28
MnO	0.04	0.03	0.09	0.17
Total	99.54	98.53	98.84	99.14
LOI	0.13	0.31	0.04	0.20
Rb (ppm)	139	134	65	49
Sr (ppm)	177	148	362	323
Ba (ppm)	850	776	821	412
Zr(ppm)	158	189	389	121
Th (ppm)	12.8	12.5	5.62	4.41
U (ppm)	4.28	4.90	2.23	1.94
La(ppm)	21.5	24.5	20.1	17.8
Lu (ppm)	0.27	0.33	0.38	0.62
$\delta^{18}O$ (‰)[a]	7.8 ± 0.2(WR)	8.8 ± 0.2 (Qtz)	6.0 ± 0.2 (WR)	5.9 ± 0.2 (WR)

Major elements by WD-XRF at USGS, Denver, CO, USA (Dave Siems, analyst). All Fe as Fe_2O_3. LOI = loss on ignition. Rb, Sr, Ba, Zr by ED-XRF at USGS, Denver, CO (Dave Siems, analyst). Th, U, La, Lu by INAA at USGS, Denver, CO (Jim Budahn, analyst).

[a]WR = Whole rock; Qtz = analysis of quartz separate. Oxygen isotope analyses by Peter Larson (Washington State University).

the Glass Mountain flow resided in the shallow crust (< 6 km) prior to final ascent and eruption [11], these granitoid xenoliths must have been quarried from relatively shallow depths. However, only hydrothermally altered granitoids (one with a U–Pb age of 330 ± 25 ka) have been found in geothermal drillholes, which extend down to about 3 km depths [12]. We therefore conclude that these fresh granitoid xenoliths were located below the hydrothermally altered rocks, at ~3 to 6 km depths, prior to their final ascent to the surface.

All the granitoid xenoliths (Table 1) are unaltered, fine to medium grained, intrusive rocks. Sample *CraterGlass 1* (CG1) is a 20 cm diameter, composite xenolith of orthopyroxene bearing granodiorite (CG1-a) and diorite (CG1-b) from one of the Crater Glass Flows, the most northeastern domes emplaced during the 1065 ± 90 yr rhyolitic Little Glass Mountain eruption [8]. Both samples are fine grained, anhedral granular, plagioclase-rich rocks that show incipient melting around crystal boundaries. Such melting almost certainly occurred immediately prior to and during transport of the xenolith to the surface during eruption. Sample *Medicine Dacite 1* (MD1) is an unmelted biotite bearing, anhedral granular granite with a partially granophyric (intergrown) groundmass. It was found within the Medicine dacite flow, which erupted about 2000 yr [8], ca. 3 km SE of the Crater Glass Flows. Sample MD2, also from the Medicine dacite flow, is an unmelted, porphyritic granite with a microcrystalline groundmass and biotite reacted to form Fe-oxide. Major and trace element compositions of the xenoliths (Table 1) and Sr, Pb and O isotopic analyses are consistent with an origin of these granitoids as part of the MLV magmatic system [4]. The crystallization of the xenolith-forming magmas heretofore has not been linked with specific eruptive episodes.

All of the xenoliths contain alkali feldspar, found as small phenocrysts and as a groundmass phase. No form of K-feldspar is present as a phenocryst in any volcanic rocks of MLV. Therefore, the K-feldspar is a late crystallizing phase present in these intrusive rocks. X-ray diffraction indicates that the feldspar is likely a sanidine cryptoperthite, with incipient unmixing that is not visible under microscopic examination. It is possible that a more ordered form of K-feldspar was present prior to re-heating and eruption, and was annealed to form the sanidine.

3. U–Th dating

Plausibly, these granitoid xenoliths could have been older than MLV (> ~0.5 Ma), with zircon cores inherited from Sierra- or Klamath basement rocks that are hypothesized to underlie MLV [13]. However, reconnaissance U–Pb analyses of zircons with the SHRIMP-RG indicate very little in situ formation of ^{206}Pb, so that they fall below the 150 ka chord on a conventional Tera-Wasserburg diagram [12].

In order to determine crystallization ages more precisely, the zircons were analyzed for U and Th nuclide abundances. ^{230}Th is a daughter product of ^{238}U with $T_{1/2} = 75$ kyr. Daughter and parent are in secular equilibrium when their abundances are inversely proportional to their half-lives. When a daughter is fractionated from its parent, e.g. during crystallization of zircon from a melt, a discrete period of time (~five half-lives; 375 ka for ^{230}Th) must elapse before secular equilibrium is re-attained [14]. Prior to that time, one may date the crystal by taking advantage of zonal variations in U/Th. These variations (Fig. 1) can cause different sectors within the grains to produce ^{230}Th at different rates. If the zircon crystallized rapidly, the sectors could form a linear isochron on a plot of (^{238}U)/(^{232}Th) versus (^{230}Th)/(^{232}Th), with slope proportional to crystal age [15] and an intercept to the equiline, the line representing secular equilibrium, equal to the initial (^{230}Th)/(^{232}Th) of the crystal (and presumably magma).

4. Analytical techniques and data reduction

We used standard mineral separation techniques to isolate zircon crystals from the xenoliths. Zircons were mounted in epoxy, polished, photographed in reflected light and imaged with

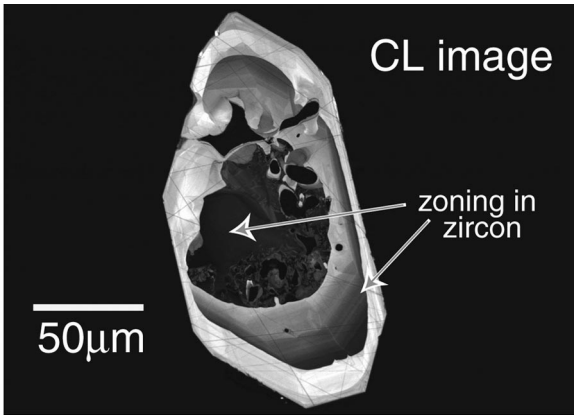

Fig. 1. CL image of crystal MD1–10. Dark zones correspond to areas higher in U (Table 2). U–Th systematics indicate a slightly younger age for the rim, compared to the core (see text and tables).

a scanning electron microscope using a cathodoluminescence (CL) detector. The mount was acid-rinsed, coated with 100 nm of Au and left in the SHRIMP-RG sample chamber overnight to reach full vacuum. Using a 30 nA $^{16}O^-$ or $^{16}O_2^-$ primary ion beam, a 50×70 μm sized rectangular region was rastered for 2 min to remove the Au coat and any surface contamination. Afterwards, a flat-floored 25×37 μm elliptical pit ($\sim$2 μm deep) was excavated into the zircon, resulting in liberation of $\sim$4–6 ng of sample that was sent as positive secondary ions to the mass spectrometer. Data were collected in 10 scans per point for $^{90}Zr_2^{16}O$, $^{230}Th^{16}O$, ^{232}Th, $^{232}Th^{16}O$, ^{234}U, ^{238}U, $^{234}U^{16}O$ and $^{238}U^{16}O$ with count times per scan ranging from 2 to 15 s for each peak. Results for the oxides were converted to an atomic basis through $^{232}Th/^{238}U = 1.11\times ThO^+/UO^+$ [16]. Standard analysis and protocols followed those in [2].

Data were collected during three analytical sessions, allowing re-polishing and Au coating of the samples in between. Repeated analyses on five individual grains yielded isochrons ([2]; Fig. 2). The isochrons were calculated with ISOPLOT [17,18] and errors are reported as 2σ uncertainties. We also determined model ages [1] by calculating two-point isochrons between the analyzed spot and an assumed initial $(^{230}Th)/(^{232}Th)$ of 1.050 ± 0.363. This value represents the weighted mean of the intercepts of the five isochrons shown in Fig. 2, plus intercepts of best fits for the multiple grains analyzed in MD2, MD1 (without MD1–3 and MD1–10), CG1a-2, CG1b-15 and CG1b-5. Using just the isochrons shown in Fig. 2, the weighted mean intercept is 1.01 ± 0.52, changing the calculated model ages at the most by only a few relative percent. These intercepts are consistent with whole rock values of lavas and granitoid xenoliths from MLV [19]. Model ages were calculated by:

$$t = \frac{-\ln(1-m)}{\lambda} \tag{1}$$

where λ is the decay constant for ^{230}Th, 9.217×10^{-6} yr^{-1}, and m is the slope of the line connecting the analyzed datum and the assumed intercept, i.e.

$$m = \frac{y-c}{x-c} \tag{2}$$

where x and y are the $(^{238}U)/(^{232}Th)$ and $(^{230}Th)/(^{232}Th)$ for the analyzed spot and c is the intercept with the equiline (1.050). Calculation of the error for the model age (σ_t) thereby requires propagation of all errors related to y, x and c according to Eqs. 4–9 of Bevington [20]. We then derive:

$$\sigma_t = \frac{1}{\lambda}\frac{1}{(x-y)(x-c)}\Big[(y-c)^2\sigma_x^2 + (x-c)^2\sigma_y^2 + (x-y)^2\sigma_c^2\Big]^{1/2} \tag{3}$$

where $\sigma_c = 1\sigma$ uncertainty on the intercept (0.363); λ is as above, and x, y, σ_x and σ_y are the $(^{238}U)/(^{232}Th)$ and $(^{230}Th)/(^{232}Th)$ and their relevant 1σ errors as analyzed. The $(^{234}U)/(^{238}U)$ of all spots was taken as unity, an assumption verified by direct measurement. Weighted means and errors were calculated according to Eqs. 5-6 and Eqs. 5-10 of Bevington [20]. U and Th concentrations (in ppm by weight) were quantified by comparing counts of $^{90}Zr_2^{16}O$ to either ^{238}U or $^{232}Th^{16}O$ for the sample relative to the standard SL13 (572 Ma), assumed to have homogeneous U and Th concentration of 238 and 21 ppm, respectively [21].

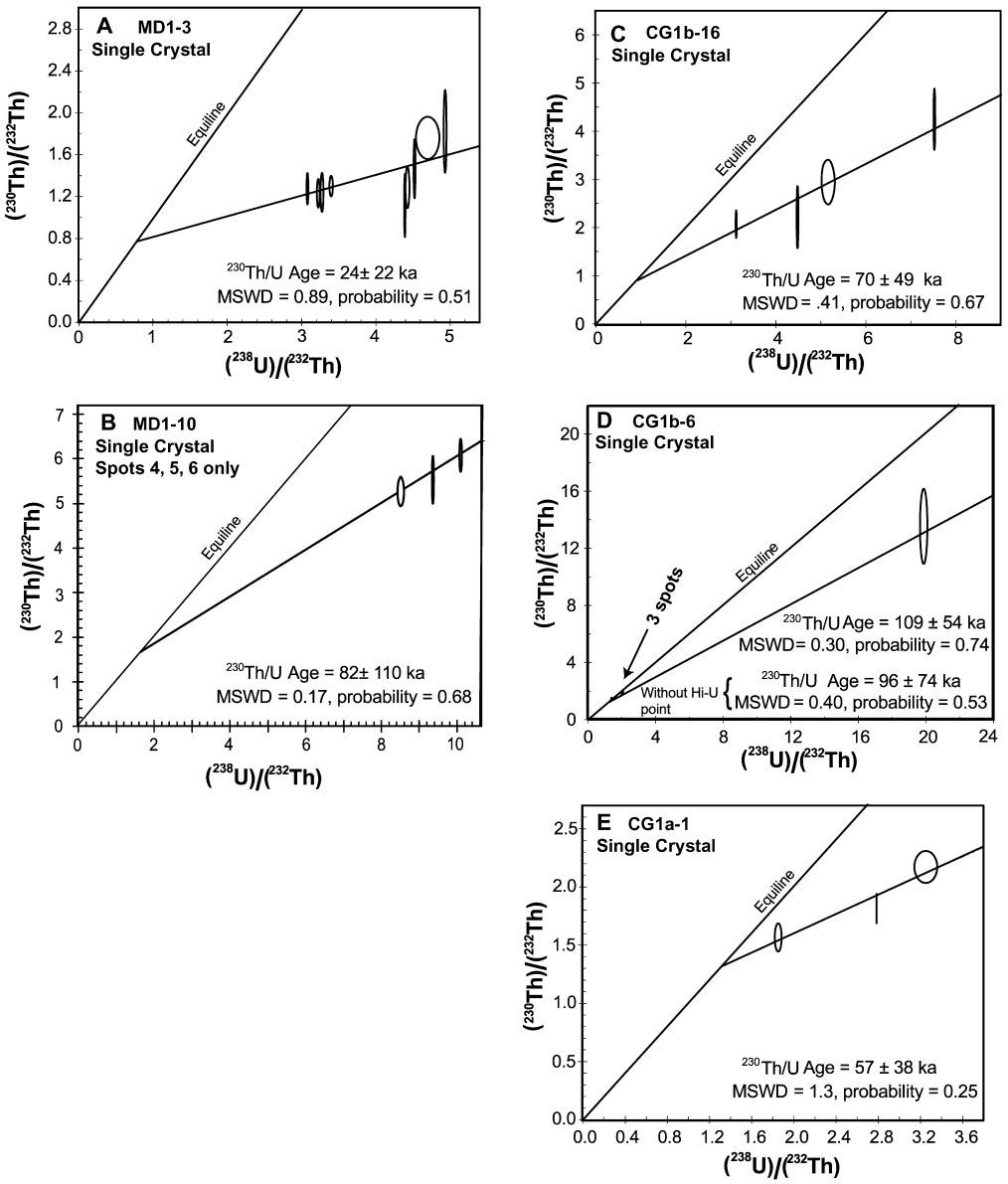

Fig. 2. (A)–(E) Plots of $(^{238}U)/(^{232}Th)$ versus $(^{230}Th)/(^{232}Th)$ for single zircon crystals from granitoid xenoliths in silicic lava flows at MLV. Trends through the data represent least-squared regressions (with MSWD and probability of fit) as calculated by ISOPLOT [17,18]. The age is calculated from the slope of the regression line and the reported error is 2σ. However, error ellipses represent 1σ analytical uncertainties.

Ar–Ar step-heating experiments were performed on K-feldspar and plagioclase separates from CG1a, MD-1 and another sample from the Medicine dacite flow, according to methods outlined in [22].

5. Results

Data were collected during three analytical sessions, allowing re-polishing and Au coating of the samples in between. Repeated analyses on five

Table 2
Analytical data, concentrations and ages of individual spots from zircon crystals

Spot #	$(^{238}U)/(^{232}Th)+1\sigma$	$(^{230}Th)/(^{232}Th)+1\sigma$	U[a] (ppm)	Th[a] (ppm)	Model age (ka)	Error (ka)
CG1a-1.1	1.866 ± 0.024	1.576 ± 0.096	2300	3800	112.3	60.5
CG1a-1.2	2.781 ± 0.003	1.826 ± 0.106	1600	1800	64.5	25.8
CG1a-1.3	3.242 ± 0.088	2.186 ± 0.111	2600	2500	79.2	21.8
CG1a-2.1	11.134 ± 0.153	7.384 ± 0.454	1900	500	107.3	14.0
CG1a-2.2	5.846 ± 0.011	3.177 ± 0.386	900	500	63.6	17.7
CG1a-3.2	5.634 ± 0.022	3.643 ± 0.408	600	300	90.5	23.9
CG1a-4.1	3.468 ± 0.009	2.485 ± 0.173	1100	1000	97.7	25.1
CG1b-5.2	5.330 ± 0.008	3.626 ± 0.476	500	300	99.9	31.7
CG1b-5.3	6.326 ± 0.103	5.269 ± 0.967	200	100	174.4	99.9
CG1b-5.4	4.125 ± 0.010	3.268 ± 0.469	400	300	138.6	60.7
CG1b-5.5	4.896 ± 0.017	2.819 ± 0.866	300	200	66.9	46.4
CG1b-6.2	2.231 ± 0.002	1.788 ± 0.086	1900	2600	106.3	39.4
CG1b-6.3	2.309 ± 0.002	1.918 ± 0.103	1600	2100	126.9	42.4
CG1b-6.4	1.648 ± 0.001	1.486 ± 0.059	2300	4700	141.8	76.9
CG1b-6.5	19.84 ± 0.167	13.612 ± 2.179	600	200	119.8	38.0
CG1b-15.1	3.064 ± 0.021	2.393 ± 0.288	800	800	119.2	50.6
CG1b-15.2	4.281 ± 0.021	2.919 ± 0.250	700	500	93.7	23.4
CG1b-16.1	4.461 ± 0.010	2.230 ± 0.526	500	300	46.1	28.1
CG1b-16.2	7.511 ± 0.012	4.253 ± 0.527	1100	500	74.3	18.6
CG1b-16.3	3.113 ± 0.005	2.078 ± 0.234	700	700	74.9	31.1
CG1b-16.4	5.161 ± 0.118	2.949 ± 0.373	1100	700	67.2	20.8
MD2–1.3	3.337 ± 0.007	1.875 ± 0.176	1100	1100	48.5	21.6
MD2–2.2	2.925 ± 0.003	1.466 ± 0.171	1100	1200	27.2	24.6
MD2–3.2	4.847 ± 0.014	1.614 ± 0.485	400	200	17.5	19.3
MD2–4.2	3.223 ± 0.013	1.254 ± 0.088	2000	2000	10.7	18.8
MD2–5.2	3.757 ± 0.007	1.345 ± 0.147	1300	1100	12.5	16.0
MD2–6.2	4.839 ± 0.008	0.673 ± 0.441	700	900	-10.3	15.5
MD2–7.2	3.671 ± 0.004	1.519 ± 0.120	2500	2100	21.4	16.2
MD2–8.3	2.005 ± 0.006	1.278 ± 0.042	7900	12400	29.7	41.7
MD2–9.1	3.852 ± 0.007	2.259 ± 0.176	1600	1300	61.2	18.5
MD2–10.1	2.260 ± 0.002	1.272 ± .0.069	4800	6700	22.5	33.4
MD2–11.1	4.346 ± 0.008	1.991 ± 0.226	1300	900	36.6	15.8
MD2–12.1	3.322 ± 0.004	1.475 ± 0.135	1500	1400	22.5	19.1
MD2–13.1	4.285 ± 0.950	1.397 ± 0.527	1100	800	12.3	23.6
MD1–1.2	5.575 ± 0.106	2.797 ± 0.503	300	200	52.9	21.6
MD1–3.2	4.510 ± 0.008	1.471 ± 0.235	900	600	14.1	14.1
MD1–3.3	3.289 ± 0.018	1.241 ± 0.153	1600	1700	9.7	19.4
MD1–3.4	4.685 ± 0.135	1.773 ± 0.166	1100	800	24.1	12.5
MD1–3.5	3.407 ± 0.019	1.311 ± 0.084	1700	1700	12.7	17.3
MD1–3.6	4.419 ± 0.023	1.290 ± 0.165	1100	900	8.0	13.0
MD1–3.7	3.235 ± 0.007	1.235 ± 0.108	1500	1400	9.6	19.0
MD1–3.8	4.913 ± 0.016	1.834 ± 0.321	700	500	24.6	15.2
MD1–3.9	4.379 ± 0.008	1.111 ± 0.263	900	600	2.0	14.7
MD1–3.10	3.090 ± 0.004	1.282 ± 0.126	1400	1500	13.1	20.7
MD1–6.2	2.857 ± 0.012	1.710 ± 0.114	2900	3200	49.5	24.3
MD1–10.2	22.464 ± 0.050	16.290 ± 0.482	4600	1800	134.9	8.7
MD1–10.3	14.690 ± 0.106	9.270 ± 0.266	5400	1300	100.1	6.2
MD1–10.4	10.045 ± 0.016	6.135 ± 0.269	2200	800	90.4	8.7
MD1–10.5	8.495 ± 0.069	5.309 ± 0.281	1300	500	92.1	11.0
MD1–10.6	9.340 ± 0.016	5.561 ± 0.436	1400	500	85.2	13.4
MD1–10.7	9.650 ± 0.850	7.379 ± 0.266	4600	1500	144.5	13.8

Table 2 (*continued*)

Spot #	$(^{238}U)/(^{232}Th)+1\sigma$	$(^{230}Th)/(^{232}Th)+1\sigma$	U[a] (ppm)	Th[a] (ppm)	Model age (ka)	Error (ka)
MD1–11.2	3.178 ± 0.015	1.442 ± 0.073	2000	2000	22.1	19.1
MD1–12.2	5.061 ± 0.108	1.607 ± 0.330	600	400	16.2	14.3
MD1–17.1	4.891 ± 0.242	1.947 ± 0.368	400	300	28.9	17.1
MD1–18.1	4.889 ± 0.041	2.033 ± 0.289	500	300	32.1	15.0
MD1–19.1	4.808 ± 0.007	2.075 ± 0.243	500	300	34.5	14.2

[a]Concentrations are rounded to the nearest 100 ppm.

individual grains yielded isochrons (Fig. 2). Three crystals from CG1 have dates of 57 ± 38 ka, 70 ± 49 ka and 109 ± 54 ka (all isochrons shown with 2σ errors), whereas the eruption age of the host lava is 1065 ± 90 yr. The isochrons for CG1 intersect the equiline at activity ratios between 1.00 and 1.34, similar to values found for whole rock lavas and xenoliths from MLV [19]. One zircon grain from sample MD1 has a crystallization age of 24 ± 22 ka (Fig. 2A), in comparison to an eruption age of 2 ka for the host Medicine dacite flow. Six spots were analyzed on MD1–10 (Fig. 1); a best-fit line through the data has a negative intercept and a poor probability of fit. However, an isochron for three spots on the rim yields an age of 82 ± 110 ka with a good probability of fit (0.68), a MSWD of 0.17 and an intercept of 1.70 ± 9.95 (Fig. 2B). Two spots in the core (spots #2 and #3) plot toward the equiline from this isochron and at higher $(^{238}U)/(^{230}Th)$. Evidently, a young rim grew around an older (~140 ka) core, as has been found for young zircons from the Taupo Volcanic Zone [23]. No other zircons were found to have rims with ages that are statistically different than their corresponding cores.

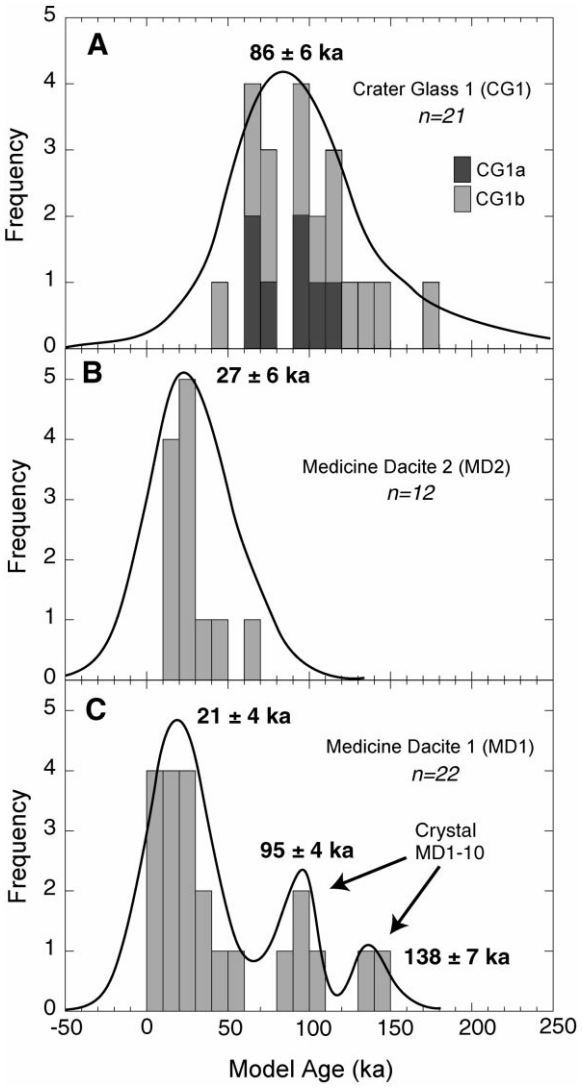

Fig. 3. Cumulative probability histograms for model ages of individual zircons from (A) CG1, (B) MD2 and (C) MD1. Zircons within CG1 and MD2 have weighted mean ages of ~86 and ~27 ka, respectively. In (C), all except grain MD1 are fitted to a single peak with weighted mean of 21 ± 4 ka (31 ± 6 ka without nine analyses of MD1–3). Grain MD1–10 forms two peaks, presumably because the rim crystallized later than the core (see text). The cumulative probability distributions represent the summation of Gaussian curves for each analysis and its associated error, all normalized so that the area beneath the final curve is equal to *n*, the number of analyses.

Zircon model ages for individual spots [1] ranged from 174 to <10 ka, consistent with the single crystal isochrons (Table 2). Model ages for zircons from the two rock types within CG1 are indistinguishable (Fig. 3A), and are older than nearly all grains from the two MD xenoliths. Given the relatively large analytical errors relative to zircon age (Table 2), it is useful to plot a cumulative probability distribution, where the Gaussian curves for all analyzed spots are overlapped to form one or more peaks (Fig. 3). Though the variation in zircon ages is large, the cumulative probability distribution indicates that the zircons from CG1 are best interpreted as having a single age with a weighted mean of 86 ± 6 ka (Fig. 3A and Table 3; all model ages and means reported with 1σ error). A single peak with identical age was also obtained using the computer program MIX [24], which uses the statistics of mixture modelling to identify multiple age populations within a group of zircons. The 86 ± 6 ka age overlaps that of the three isochrons for CG1. Moreover, the 1σ errors for all but three spots overlap the weighted mean (and all 2σ errors overlap). We conclude that none of the CG1 zircon ages is statistically different than the mean age for that sample.

Model ages for zircons from MD2 are all <70 ka and give a weighted mean of 27 ± 6 ka and a single peak in Fig. 3B. Most of the zircons from the other Medicine dacite xenolith MD1, have a similar young age. The xenoliths from Medicine dacite are therefore younger than those studied from the Crater Glass flow. Model ages for spots from seven of the analyzed crystals from MD1 have a weighted mean of 31 ± 6 ka. By including the nine analyses of crystal MD1–3, an age of 21 ± 4 ka is obtained. A single zoned crystal, MD1–10 is responsible for the two older peaks in Fig. 3C and the older isochron (Fig. 2B). Once again, MIX [24] corroborated the three peaks and ages shown within the cumulative probability distribution for sample MD1 (Fig. 3C).

Above, we have chosen to calculate weighted means for the zircon analyses rather than to report a spread of ages for each xenolith. With the exception of a single zircon (MD1–10), all analyses and their error bars fall within the 2σ uncertainty of the mean age for their host xenolith. Thus, differences between ages of individual grains (or growth zones) within each xenolith are not statistically significant. Certainly there must have been a discrete time interval over which the zircons crystallized, but it currently cannot be defined precisely. With future improvements in the spatial resolution and sensitivity of ion microprobes, one might delineate a more exact time interval over which these xenoliths crystallized.

Table 3
Summary of U–Th results

Sample	Pooled model ages (ka $\pm 1\sigma$)	Isochron age (ka $\pm 2\sigma$)	# Spots	# Grains	Intercept w/equiline ($\pm 1\sigma$)
Single crystals					
MD1–3	14 ± 5	24 ± 22	9	1	0.762 ± 0.752
MD1–10	103 ± 4	–	6	1	–
MD1–10 (rim)	90 ± 6	82 ± 110	3	1	1.70 ± 9.95
CG1b-16	67 ± 12	70 ± 49	4	1	1.019 ± 2.126
CG1b-6	119 ± 22	109 ± 54	4	1	1.172 ± 1.114
CG1a-1	76 ± 16	57 ± 38	3	1	1.022 ± 0.288
Multiple crystals[a]					
CG1a+b	86 ± 6	–	21	8	
MD2	27 ± 6	–	12	12	1.075 ± 0.567
MD1	31 ± 6	–	7	7	1.159 ± 1.210

[a]CG1a+b and MD2 multiple crystal averages include all crystals from those samples. MD1 multiple crystal average does not include MD1–10 or MD1–3. Weighted mean for MD1 including MD1–3 is 21 ± 4 ka.

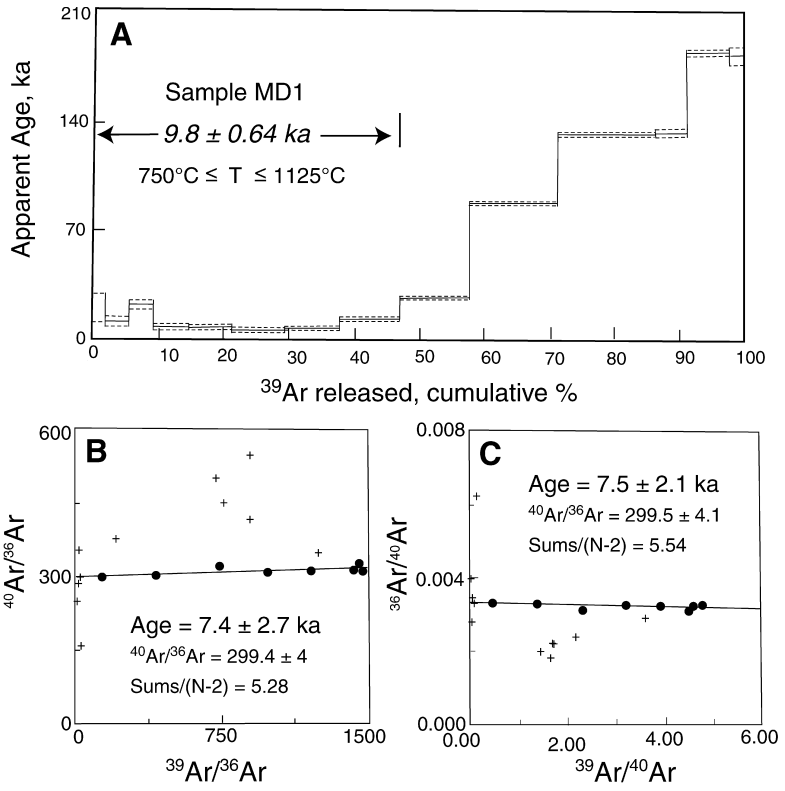

Fig. 4. Ar–Ar data for a K-feldspar separate from sample MD1. (A) Ar released between 825 and 1125°C gives a plateau at ~10 ka. The rock was likely partially reset from an older age during eruption. Higher temperature steps may 'remember' such an earlier crystallization event. Isochron (B) and inverse isochron (C) plots show the data for the 750–1125°C steps as filled circles, which form isochrons indicating ages of ~7.5 ka and intercepts within error of the $^{40}Ar/^{36}Ar$ ratio of atmospheric Ar. The plus symbols denote the higher temperature steps that were not included in the plateau shown in (A). Errors are 1σ.

6. Intrusive episodes beneath MLV

At least two episodes of granitoid magmatism are evident (Fig. 3 and Table 3). One episode, represented by CG1, suggests intrusion at 86 ± 6 ka beneath the site of the present day Crater Glass Flows. Granitic magma also intruded 20–30 ka beneath the subsequent site of the Medicine dacite flow (MD1 and MD2). A single crystal found within MD1 is older than all others, with a core that crystallized ~140 ka, and a younger rim (~95 ka). The grain may be derived from an earlier intrusion that was partially assimilated during subsequent magmatism.

Both the isochrons and the model ages are useful in unraveling the history of magmatism. The isochrons of single crystals differentiate age populations within a single unit or crystal (e.g. MD1–10) and permit independent inference of the initial $(^{230}Th)/(^{232}Th)$ of the zircons. The fact that multiple analyses of an individual zircon can form an isochron implies that the entire grain crystallized over a relatively limited time interval. When individual zircons or zircon separates are nearly uniform in age, the data can be pooled so that different spots are weighted by the magnitude of their analytical uncertainties, thereby minimizing the leverage of analyses with large errors. This results in weighted mean ages with relatively small estimated errors (Table 3 and Fig. 3).

The zircon ages are older than $^{40}Ar/^{39}Ar$ (Ar–Ar) dates on K-feldspar from the same xenoliths. For example, K-feldspar from CG1 yielded identical isochron and inverse isochron ages of

17.0 ± 1.6 ka, about 70 000 years younger than the pooled zircon model age (plateau age of 20.6 ± 0.6 ka). Likewise, MD1 has a plateau age of 9.8 ± 0.6 ka and isochron and inverse isochrons of about 7.5 ± 2.4 ka, relative to zircon ages some 10–20 thousand years older (Fig. 4). An age spectrum for a plagioclase separate from MD1 gave an identical result. The younger Ar–Ar ages are explained by heating of the xenolith and partial degassing of radiogenic Ar during eruption. The stable plateaus and linear isochrons for these samples (Fig. 4) therefore provide only minimum estimates of crystallization age (i.e. the samples were partially, but not totally re-set during eruption, or they would have yielded ages of 1–2 ka). For CG1, the feldspar groundmass had crystallized during or after zircon crystallization, but before 17 ka. Subsequently, the rock remained crystalline until eruption 1065 ± 90 yr, when it was partially reset. Similarly, MD1 and MD2 must have cooled below their solidi, and stayed there, between ~20–30 ka (zircon ages) and 7 ka (Ar–Ar age). We have opted not to interpret the Ar spectra in terms of cooling through an estimated closure temperature for the host mineral phase [25], because we know neither the rate of cooling nor structural state of the feldspar prior to final re-heating and eruption. Therefore, we conservatively interpret the Ar data as minimum (youngest possible) crystallization ages for the feldspars.

Neither the Ar–Ar nor U–Th ages (Fig. 5) provide any record of pre-MLV (including Mesozoic) basement inferred to exist beneath the volcano [13]. Either the granitoids were generated by melting of pre-MLV basement without preserving any

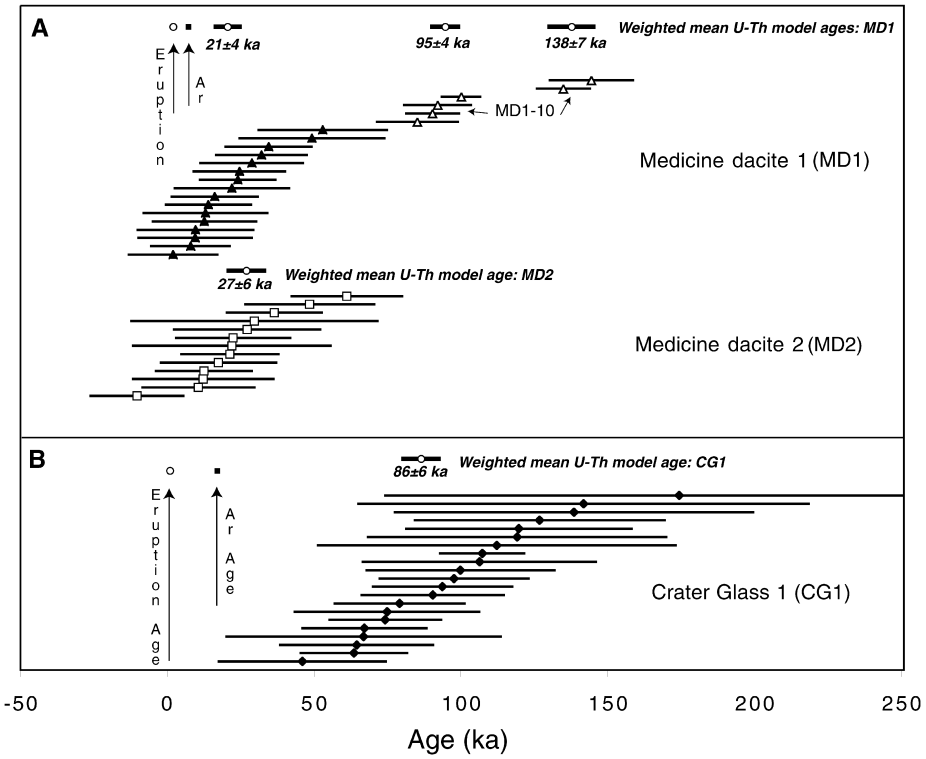

Fig. 5. U–Th model ages for all analyzed spots plus their 1σ error bars. Vertically, the zircon ages are arranged by relative age and by eruptive unit. The Ar–Ar ages for the granitoid xenoliths were partially re-set during eruption in the late Holocene. (A) The two samples from the Medicine dacite flow are both young, with mean zircon ages <30 ka. One crystal (MD1–10) is older, with a rim interpreted to be younger than its core (Fig. 3C). (B) The sample from Crater Glass flow is interpreted to have a single age of 86 ± 6 ka.

relict zircons, or they crystallized from young intermediate-to-silicic melts related to MLV and its underlying Pleistocene-aged crust [4].

In either scenario, granitoid intrusion coincided with two brief but voluminous episodes of mafic volcanism at MLV, approximately 90 and 30 ka, respectively. More than 15 km^3 of basaltic lava vented in three eruptions between 97 and 85 ka and now cover over half of the southeast and east flanks of the volcano. The basalt of Mammoth Crater and andesite of Indian Butte were erupted between 20 and 36 ka (Donnelly-Nolan and Lanphere, in preparation). The intermediate to silicic granitoids thus may represent melts of young crust that formed due to high-heat flux during episodes of abundant mafic volcanism [9,11,26]. Limited rhyolitic and dacitic volcanism between 85 and 10 ka indicates that little of this silicic magma reached the surface. Only one rhyolite was erupted during this time, the $\sim$30 ka rhyolite of Mt. Hoffman, and it does not correlate well with MD1 or MD2 (e.g. $\delta^{18}O$ of 5.5 WR and 6.3 (plagioclase) compared with the much higher values for those two xenoliths; [10], Table 1). Similarly, no dacitic or andesitic eruptive units correlate with CG1a and b.

7. Summary

This study shows that $<$100 ka zircons may be successfully dated by U–Th techniques, and that even very young magmatic events can be differentiated (i.e. 25 versus 90 ka). Multiple analyses of individual grains are particularly useful, as they can provide detailed histories of zircon growth. Moreover, if such growth is rapid, the multiple analyses permit dating using isochron techniques. Our results also reveal periods of silicic magmatism at MLV that were not indicated by surface volcanism, and allowed us to piece together part of the plutonic history of the volcano. Because subvolcanic intrusions can control the distribution of subsequent lavas [2], host ore bodies [27], power hydrothermal systems, and when melted, can modify the chemical and isotopic composition of ascending lavas [11,26,28], they have an integral role in the architecture and dynamics of magmatic systems. Grain-by-grain studies of zircon and other minerals will be a critical tool in unraveling the complex history of volcanoes and their underlying intrusions.

Acknowledgements

C. Holdsworth separated zircons from the granitoid xenoliths and R. Oscarson helped with CL imaging. J.Y. Saburomaru assisted with the Ar–Ar analyses. We appreciate advice, encouragement and a review from C. Bacon. Careful reviews were also done by P. Lipman, M. Reagan and T. Sisson. We thank EPSL reviewers M. Dungan, O. Sigmarsson and G. Zellmer, whose input helped improve the manuscript. CalEnergy Corp. provided information about geothermal drillholes and access to downhole samples. The work was funded primarily by the USGS Volcano Hazards Program with additional support from the US DOE National Geothermal Program.*[AH]*

References

[1] M.R. Reid, C.D. Coath, T.M. Harrison, K.D. McKeegan, Prolonged residence times for the youngest rhyolites associated with Long Valley Caldera: ^{230}Th-^{238}U ion microprobe dating of young zircons, Earth Planet. Sci. Lett. 150 (1997) 27–39.

[2] C.R. Bacon, H.M. Persing, J.L. Wooden, T.R. Ireland, Late Pleistocene granodiorite beneath Crater lake caldera, Oregon, dated by ion microprobe, Geology 28 (2000) 467–470.

[3] G. Capaldi, R. Pece, On the reliability of the ^{230}Th-^{238}U dating method applied to young volcanic rocks, J. Volcanol. Geotherm. Res. 11 (1981) 367–372.

[4] S.A. Mertzman, R.J. Williams, Genesis of Recent silicic magmatism in the Medicine Lake Highland, California: evidence from cognate inclusions found at Little Glass Mountain, Geochim. Cosmochim. Acta 45 (1981) 1463–1478.

[5] J.B. Lowenstern, M.A. Clynne, T.D. Bullen, Comagmatic A-type granophyre and rhyolite from the Alid volcanic center, Eritrea, northeast Africa, J. Petrol. 12 (1997) 1707–1721.

[6] S.J.A. Brown, R.M. Burt, J.W. Cole, S.J.P. Krippner, R.C. Price, I. Cartwright, Plutonic lithics in ignimbrites of Taupo Volcanic Zone, New Zealand; sources and conditions of crystallization, Chem. Geol. 148 (1998) 21–41.

[7] R.M. Burt, S.J.A. Brown, J.W. Cole, D. Shelly, T.E. Wright, Glass-bearing plutonic fragments from ignimbrites of the Okataina caldera complex, Taupo Volcanic Zone, New Zealand: remnants of a partially molten intrusion associated with preceding eruptions, J. Volcanol. Geotherm. Res. 84 (1998) 209–237.
[8] J. Donnelly-Nolan, D.E. Champion, C.D. Miller, T.L. Grove, D.A. Trimble, Post-11,000-year volcanism at Medicine Lake volcano, Cascade range, northern California, J. Geophys. Res. 95 (1990) 19,693–19,704.
[9] J.M. Donnelly-Nolan, A magmatic model of Medicine Lake volcano, California, J. Geophys. Res. 93 (1988) 4412–4420.
[10] J. Donnelly-Nolan, Abrupt shift in $\delta^{18}O$ values at Medicine Lake volcano (California, USA), Bull. Volcanol. 59 (1998) 529–536.
[11] T.L. Grove, J.M. Donnelly-Nolan, T. Housh, Magmatic processes that generated the rhyolite of Glass Mountain, Medicine Lake volcano, N. California, Contrib. Miner. Petrol. 127 (1997) 205–223.
[12] J.B. Lowenstern, J.L. Wooden, M. Lanphere, H.M. Persing, J. Donnelly-Nolan, T.L. Grove, Late Quaternary U-Pb and Ar-Ar ages of granitic intrusions beneath Medicine Lake volcano, California, USA, EOS 80 (1999) F1130.
[13] G.S. Fuis, J.J. Zucca, W.D. Mooney, B. Milkereit, A geologic interpretation of seismic-refraction results in northeastern California, Geol. Soc. Am. Bull. 98 (1987) 53–65.
[14] J.B. Gill, D.M., Pyle, R.W. Williams, Igneous rocks, in: M. Ivanovich, R.S. Harmon (Eds.), Uranium Series Disequilibrium: Applications to Earth, Marine and Environmental Sciences, Clarendon Press, Oxford, 1992, pp. 207–258.
[15] C.L. Allegre, ^{230}Th dating of volcanic rocks: a comment, Earth. Planet. Sci. Lett. 5 (1968) 209–210.
[16] T.R. Ireland, Ion microprobe mass spectrometry: techniques and applications in cosmochemistry, geochemistry and geochronology, in: H. Hyman, M. Rowe (Eds.) Advances in Analytical Geochemistry, JAI Press, Greenwich, 1995, pp. 1–118.
[17] K.R. Ludwig, Isoplot: a plotting and regression program for radiogenic-isotope data, Version, 2.53, US Geological Survey Open File Report 91–445, 1991.
[18] K.R. Ludwig, D.M. Titterington, Calculation of $^{230}Th/U$ isochrons, ages and errors, Geochim. Cosmochim. Acta 58 (1994) 5031–5042.
[19] J.V. Hill, M.K. Reagan, J. Donnelly-Nolan, U-series systematics of Glass Mountain Lavas, the Medicine Lake Highlands, Northcentral California, EOS 70 (1989) 1388.
[20] P.R. Bevington, Data Reduction and Error Analysis for the Physical Sciences, McGraw-Hill, New York, 1969.
[21] W. Compston, I.S. Williams, C.E. Meyer, U–Pb geochronology of zircons from lunar breccia 73217 using a sensitive high mass-resolution ion probe, J. Geophys. Res. 89 (Suppl.) (1984) B525–B534.
[22] M.A. Lanphere, Comparison of conventional K–Ar and $^{40}Ar/^{39}Ar$ dating of young mafic volcanic rocks, Quat. Res. 53 (2000) 294–301.
[23] S.J.A. Brown, I.R. Fletcher, SHRIMP U–Pb dating of the preeruption growth history of zircons from the 340 ka Whakamaru Ignimbrite, New Zealand: Evidence for >250 ky magma residence times, Geology 27 (1999) 1035–1038.
[24] M.S. Sambridge, W. Compston, Mixture modeling of multi-component data sets with application to ion-probe zircon ages, Earth Planet. Sci. Lett. 128 (1994) 373–390.
[25] T.M. Harrison, I. McDougall, The thermal significance of potassium feldspar K–Ar ages inferred from $^{40}Ar/^{39}Ar$ age spectrum results, Geochim. Cosmochim. Acta 46 (1982) 1811–1820.
[26] R.J. Kinzler, J.M. Donnelly-Nolan, T.L. Grove, Late Holocene hydrous mafic magmatism at the Paint Pot Crater and Callahan flows, Medicine Lake volcano, N. California and the influence of H_2O in the generation of silicic magmas, Contrib. Miner. Petrol. 138 (2000) 1–16.
[27] J.W. Hedenquist, J.B. Lowenstern, The role of magmas in the formation of hydrothermal ore deposits, Nature 370 (1994) 519–527.
[28] S. Nakada, C.R. Bacon, A.E. Gartner, Origin of phenocrysts and compositional diversity in pre-Mazama rhyodacite lavas, Crater lake, Oregon, J. Petrol. 35 (1994) 127–162.